Research Article

Peristaltic Flow of a Magneto-Micropolar Fluid: Effect of Induced Magnetic Field

Kh. S. Mekheimer

Department of Mathematics, Faculty of Science, Al-Azhar University, Nasr City 11884, Cairo, Egypt

Correspondence should be addressed to Kh. S. Mekheimer, kh_mekheimer@yahoo.com

We carry out the effect of the induced magnetic field on peristaltic transport of an incompressible conducting micropolar fluid in a symmetric channel. The flow analysis has been developed for low Reynolds number and long wavelength approximation. Exact solutions have been established for the axial velocity, microrotation component, stream function, magnetic-force function, axial-induced magnetic field, and current distribution across the channel. Expressions for the shear stresses are also obtained. The effects of pertinent parameters on the pressure rise per wavelength are investigated by means of numerical integrations, also we study the effect of these parameters on the axial pressure gradient, axial-induced magnetic field, as well as current distribution across the channel and the nonsymmetric shear stresses. The phenomena of trapping and magnetic-force lines are further discussed.

1. Introduction

It is well known that many physiological fluids behave in general like suspensions of deformable or rigid particles in a Newtonian fluid. Blood, for example, is a suspension of red cells, white cells, and platelets in plasma. Another example is cervical mucus, which is a suspension of macromolecules in a water-like liquid. In view of this, some researchers have tried to account for the suspension behavior of biofluids by considering them to be non-Newtonian [1–6].

Eringen [7] introduced the concept of simple microfluids to characterise concentrated suspensions of neutrally buoyant deformable particles in a viscous fluid where the individuality of substructures affects the physical outcome of the flow. Such fluid models can be used to rheologically describe polymeric suspensions, normal human blood, and so forth, and have found applications in physiological and engineering problems [8–10]. A subclass of these microfluids is known as micropolar fluids where the fluid microelements are considered

to be rigid [11, 12]. Basically, these fluids can support couple stresses and body couples and exhibit microrotational and microinertial effects.

The phenomenon of peristalsis is defined as expansion and contraction of an extensible tube in a fluid generate progressive waves which propagate along the length of the tube, mixing and transporting the fluid in the direction of wave propagation. It is an inherent property of many tubular organs of the human body. In some biomedical instruments, such as heart-lung machines, peristaltic motion is used to pump blood and other biological fluids. It plays an indispensable role in transporting many physiological fluids in the body in various situations such as urine transport from the kidney to the bladder through the ureter, transport of spermatozoa in the ductus efferentes of the male reproductive tract, movement of ovum in the fallopian tubes, vasomotion of small blood vessels, as well as mixing and transporting the contents of the gastrointestinal passage.

Peristaltic pumping mechanisms have been utilized for the transport of slurries, sensitive or corrosive fluids, sanitary fluid, noxious fluids in the nuclear industry, and many others. In some cases, the transport of fluids is possible without moving internal mechanical components as in the case with peristaltically operated microelectromechanical system devices [13].

The study of peristalsis in the context of fluid mechanics has received considerable attention in the last three decades, mainly because of its relevance to biological systems and industrial applications. Several studies have been made, especially for the peristalsis in non-Newtonian fluids which have promising applications in physiology [14–23]. The main advantage of using a micropolar fluid model to study the peristaltic flow of suspensions in comparison with other classes of non-Newtonian fluids is that it takes care of the rotation of fluid particles by means of an independent kinematic vector called the microrotation vector.

Magnetohydrodynamic (MHD) is the science which deals with the motion of a highly conducting fluids in the presence of a magnetic field. The motion of the conducting fluid across the magnetic field generates electric currents which change the magnetic field, and the action of the magnetic field on these currents gives rise to mechanical forces which modify the flow of the fluid [24]. MHD flow of a fluid in a channel with elastic, rhythmically contracting walls (peristaltic flow) is of interest in connection with certain problems of the movement of conductive physiological fluids (e.g., the blood and blood pump machines) and with the need for theoretical research on the operation of a peristaltic MHD compressor. Effect of a moving magnetic field on blood flow was studied by Stud et al. [25], Srivastava and Agrawal [26] considered the blood as an electrically conducting fluid and it constitutes a suspension of red cells in plasma. Also Agrawal and Anwaruddin [27] studied the effect of magnetic field on blood flow by taking a simple mathematical model for blood through an equally branched channel with flexible walls executing peristaltic waves using long wavelength approximation method.

Some recent studies [28–41] have considered the effect of a magnetic field on peristaltic flow of a Newtonian and non-Newtonian fluids, and in all of these studies the effect of the induced magnetic field have been neglected.

The first investigation of the effect of the induced magnetic field on peristaltic flow was studied by Vishnyakov and Pavlov [42] where they considers the peristaltic MHD flow of a conductive Newtonian fluid; they used the asymptotic narrow-band method to solve the problem and only obtained the velocity profiles in certain channel cross-sections for definite parameter values. Currently, there is only two attempts [43, 44] for a study of the effect of induced magnetic field, one for a couple-stress fluid and the other for a non-Newtonian fluid (biviscosity fluid). To the best of our knowledge , the influence of a magnetic field on

peristaltic flow of a conductive micropolar fluid has not been investigate with or without the induced magnetic field.

With keeping the above discussion in mind, the goal of this investigation is to study the effect of the induced magnetic field on peristaltic flow of a micropolar fluid (as a blood model). The flow analysis is developed in a wave frame of reference moving with the velocity of the wave. The problem is first modeled and then solved analytically for the stream function, magnetic-force function, and the axial pressure gradient. The results for the pressure rise , shear stresses, the axial induced magnetic field, and the distribution of the current density across the channel have been discussed for various values of the problem parameters. Also, the contour plots for the magnetic force and stream functions are presented, the pumping characteristics and the trapping phenomena are discussed in detail. Finally, The main conclusions are summarized in the last section.

2. Mathematical modelling

Consider the unsteady hydromagnetic flow of a viscous, incompressible, and electrically conducting micropolar fluid through an axisymmetric two-dimensional channel of uniform thickness with a sinusoidal wave traveling down its wall. We choose a rectangular coordinate system for the channel with X' along the centerline in the direction of wave propagation and Y' transverse to it. The system is stressed by an external transverse uniform constant magnetic field of strength H'_0, which will give rise to an induced magnetic field $H'(h'_{X'}(X', Y', t'), h'_{Y'}(X', Y', t'), 0)$ and the total magnetic field will be $H'^+(h'_{X'}(X', Y', t'), H'_0 + h'_{Y'}(X', Y', t'), 0)$. The plates of the channel are assumed to be nonconductive, and the geometry of the wall surface is defined as

$$h'(X', t') = a + b \cos \frac{2\pi}{\lambda}(X' - ct'), \tag{2.1}$$

where a_0 is the half-width at the inlet, b is the wave amplitude, λ is the wavelength, c is the propagation velocity, and t' is the time.

Neglecting the body couples, the equations of motion for unsteady flow of an incompressible micropolar fluid are

$$\vec{\nabla} \cdot \vec{V}' = 0,$$

$$\rho \left\{ \frac{\partial \vec{V}'}{\partial t'} + \vec{V}' \cdot \vec{\nabla} \vec{V}' \right\} = -\vec{\nabla} p' + k \vec{\nabla} \times \vec{w}' + (\mu + k) \vec{\nabla}^2 \vec{V}' + \rho \vec{f}', \tag{2.2}$$

$$\rho j \left\{ \frac{\partial \vec{V}'}{\partial t'} + \vec{V}' \cdot \vec{\nabla} \vec{w}' \right\} = -2k \vec{w}' + k \vec{\nabla} \times \vec{V}' - \gamma (\vec{\nabla} \times \vec{\nabla} \times \vec{w}') + (\alpha + \beta + \gamma) \nabla (\vec{\nabla} \cdot \vec{w}'),$$

where $\vec{V}'$ is the velocity vector, $\vec{w}'$ is the microrotation vector, p' is the fluid pressure, $\vec{f}'$ is the body force, and ρ and j are the fluid density and microgyration parameter. Further, the material constants (new viscosities of the micropolar fluid) μ, k, α, β, and γ satisfy the following inequalities (obtained by Eringen [11]):

$$2\mu + k \geq 0, \quad k \geq 0, \qquad 3\alpha + \beta + \gamma \geq 0, \quad \gamma \geq |\beta|. \tag{2.3}$$

The governing equations for a magneto-micropolar fluid are as follows:
Maxwell's equations

$$\nabla \cdot \vec{H}' = 0, \qquad \nabla \cdot \vec{E}' = 0, \tag{2.4}$$

$$\nabla \wedge \vec{H}' = \vec{J}', \quad \text{with } \vec{J}' = \sigma\{\vec{E}' + \mu_e(\vec{V}' \wedge \vec{H}'^+)\}, \tag{2.5}$$

$$\nabla \wedge \vec{E}' = -\mu_e \frac{\partial \vec{H}'}{\partial t'}, \tag{2.6}$$

the continuity equation

$$\nabla \cdot \vec{V}' = 0, \tag{2.7}$$

the equations of motion

$$\rho\left\{\frac{\partial \vec{V}'}{\partial t'} + (\vec{V}' \cdot \vec{\nabla})\vec{V}'\right\} = -\nabla\left(p' + \frac{1}{2}\mu_e(H'^+)^2\right) + (\mu + k)\nabla^2\,\vec{V}' + k\vec{\nabla} \times \vec{w}' - \mu_e\,(\vec{H}'^+ \cdot \vec{\nabla})\vec{H}'^+,$$

$$\rho j\left\{\frac{\partial \vec{V}'}{\partial t'} + (\vec{V}' \cdot \vec{\nabla})\vec{w}'\right\} = -2k\vec{w}' + k\vec{\nabla} \times \vec{V}' - \gamma(\vec{\nabla} \times \vec{\nabla} \times \vec{w}') + (\alpha + \beta + \gamma)\vec{\nabla}(\vec{\nabla} \cdot \vec{w}'),$$

$$\nabla^2 = \frac{\partial^2}{\partial X'^2} + \frac{\partial^2}{\partial Y'^2}, \tag{2.8}$$

where $\vec{E}'$ is an induced electric field, $\vec{J}'$ is the electric current density, μ_e is the magnetic permeability, and σ is the electrical conductivity.

Combining (2.4) and (2.5)–(2.7), we obtain the induction equation:

$$\frac{\partial \vec{H}'^+}{\partial t'} = \vec{\nabla} \wedge \{\vec{V}' \wedge \vec{H}'^+\} + \frac{1}{\zeta}\nabla^2 \vec{H}'^+, \tag{2.9}$$

where $\zeta = 1/\sigma\mu_e$ is the magnetic diffusivity.

We should carry out this investigation in a coordinate system moving with the wave speed c, in which the boundary shape is stationary. The coordinates and velocities in the laboratory frame (X', Y') and the wave frame (x', y') are related by

$$x' = X' - ct', \qquad y' = Y',$$
$$u' = U' - c, \qquad v' = V', \tag{2.10}$$

where U', V', and u', v' are the velocity components in the corresponding coordinate systems.

Using these transformations and introducing the dimensionless variables

$$x = \frac{x'}{\lambda}, \qquad y = \frac{y'}{a}, \qquad u = \frac{u'}{c}, \qquad v = \frac{\lambda v'}{ac}, \qquad h = \frac{h'(x')}{a},$$

$$p = \frac{a^2}{\lambda \mu c} p'(x'), \qquad t = \frac{ct'}{\lambda}, \qquad j = \frac{j'}{a^2}, \qquad \psi = \frac{\psi'}{ca}, \qquad \phi = \frac{\phi'}{H_0 a},$$

(2.11)

we find that the equations which govern the MHD flow for a micropolar fluid in terms of the stream function $\psi(x, y)$ and magnetic-force function $\phi(x, y)$ are

$$\mathrm{Re}\delta\left\{\left(\psi_y \frac{\partial}{\partial x} - \psi_x \frac{\partial}{\partial y}\right)\psi_y\right\} = -\frac{\partial p_m}{\partial x} + \frac{1}{1-N}\nabla^2 \psi_y + \frac{N}{1-N}\frac{\partial w}{\partial y} + \mathrm{Re}S^2 \phi_{yy}$$

$$+ \mathrm{Re}S^2 \delta\left(\phi_y \frac{\partial}{\partial x} - \phi_x \frac{\partial}{\partial y}\right)\phi_y,$$

(2.12)

$$\mathrm{Re}\delta^3\left\{\left(\psi_x \frac{\partial}{\partial y} - \psi_y \frac{\partial}{\partial x}\right)\psi_x\right\} = -\frac{\partial p_m}{\partial y} - \frac{\delta^2}{1-N}\nabla^2 \psi_x - \frac{\delta^2 N}{1-N}\frac{\partial w}{\partial x} - \mathrm{Re}S^2\delta^2 \phi_{xy}$$

$$- \mathrm{Re}S^2\delta^3\left(\phi_y \frac{\partial}{\partial x} - \phi_x \frac{\partial}{\partial y}\right)\phi_x,$$

(2.13)

$$\mathrm{Re}\delta j\left(\frac{1-N}{N}\right)\left\{\left(\psi_y \frac{\partial}{\partial x} - \psi_x \frac{\partial}{\partial y}\right)w\right\} = -2w - \nabla^2 \psi + \left(\frac{2-N}{m^2}\right)\nabla^2 w,$$

(2.14)

$$\psi_y - \delta(\psi_y \phi_x - \psi_x \phi_y) + \frac{1}{R_m}\nabla^2 \phi = E,$$

(2.15)

where

$$u = \frac{\partial \psi}{\partial y}, \qquad v = -\delta\frac{\partial \psi}{\partial x}, \qquad h_x = \frac{\partial \phi}{\partial y}, \qquad h_y = -\delta\frac{\partial \phi}{\partial x},$$

$$\nabla^2 = \delta^2 \frac{\partial^2}{\partial x^2} + \frac{\partial^2}{\partial y^2},$$

(2.16)

and the dimensionless parameters as follows:

   (i) Reynolds number $\mathrm{Re} = ca\rho/\mu$,
  (ii) wave number $\delta = a/\lambda$,
 (iii) Strommer's number (magnetic-force number) $S = (H_0/c)\sqrt{\mu_e/\rho}$,
  (iv) the magnetic Reynolds number $R_m = \sigma\mu_e ac$,
   (v) the coupling number $N = k/(k+\mu)$ $(0 \le N \le 1)$, $m^2 = a^2 k(2\mu + k)/(\gamma(\mu + k))$ is the micropolar parameter,
  (vi) the total pressure in the fluid, which equals the sum of the ordinary and magnetic pressure, is $p_m = p + (1/2)\mathrm{Re}\delta(\mu_e(H^+)^2/\rho c^2)$, and $E(= -E/cH_0)$ is the electric field strength. The parameters α, β do not appear in the governing equations as the microrotation vector is solenoidal. However, (2.12)–(2.15) reduce to the classical MHD Navier-Stokes equations as $k \to 0$.

Excluding the total pressure from (2.12) and (2.13), we obtain

$$\text{Re}\delta\left\{\left(\psi_y\frac{\partial}{\partial x}-\psi_x\frac{\partial}{\partial y}\right)\nabla^2\psi\right\}=\frac{1}{1-N}\nabla^4\psi+\frac{N}{1-N}\nabla^2w+\text{Re}S^2\nabla^2\phi_y$$

$$+\text{Re}S^2\delta\left(\phi_y\frac{\partial}{\partial x}-\phi_x\frac{\partial}{\partial y}\right)\nabla^2\phi, \quad (2.17)$$

$$\text{Re}\delta j\left(\frac{1-N}{N}\right)\left\{\left(\psi_y\frac{\partial}{\partial x}-\psi_x\frac{\partial}{\partial y}\right)w\right\}=-2w-\nabla^2\psi+\left(\frac{2-N}{m^2}\right)\nabla^2w.$$

The instantaneous volume flow rate in the fixed frame is given by

$$Q=\int_0^{h'}U'(X',Y',t)dY', \quad (2.18)$$

where h' is a function of X' and t.

The rate of volume flow in the wave frame is given by

$$q=\int_0^{h'}u'(x',y')dy', \quad (2.19)$$

where h' is a function of x' alone. If we substitute (2.10) into (2.18) and make use of (2.19), we find that the two rates of volume flow are related through

$$Q=q+ch'. \quad (2.20)$$

The time mean flow over a period T at a fixed position X' is defined as:

$$\overline{Q}=\frac{1}{T}\int_0^T Q\,dt. \quad (2.21)$$

Substituting (2.20) into (2.21), and integrating, we get

$$\overline{Q}=q+ac. \quad (2.22)$$

On defining the dimensionless time-mean flows θ and F, respectively, in the fixed and wave frame as

$$\theta=\frac{\overline{Q}}{ac},\qquad F=\frac{q}{ac}, \quad (2.23)$$

one finds that (2.22) may be written as

$$\theta=F+1, \quad (2.24)$$

where

$$F = \int_0^h \frac{\partial \psi}{\partial y} dy = \psi(h) - \psi(0). \tag{2.25}$$

We note that h represents the dimensionless form of the surface of the peristaltic wall:

$$h(x) = 1 + \alpha \cos(2\pi x), \tag{2.26}$$

where

$$\alpha = \frac{b}{a} \tag{2.27}$$

is the amplitude ratio or the occlusion.

If we select the zero value of the streamline at the streamline $(y = 0)$

$$\psi(0) = 0, \tag{2.28}$$

then the wall $(y = h)$ is a streamline of value

$$\psi(h) = F. \tag{2.29}$$

For a non-conductive elastic channel wall, the boundary conditions for the dimensionless stream function $\psi(x, y)$ and magnetic-force function $\phi(x, y)$ in the wave frame are [42, 44]

$$\psi = 0, \quad \frac{\partial^2 \psi}{\partial y^2} = 0, \quad w = 0, \quad \frac{\partial \phi}{\partial y} = 0 \quad \text{on } y = 0,$$

$$\frac{\partial \psi}{\partial y} = -1, \quad \psi = F, \quad w = 0, \quad \phi = 0, \quad \frac{\partial \phi}{\partial y} = 0 \quad \text{on } y = h(x). \tag{2.30}$$

Under the long wavelength and low Reynolds number consideration [4–6, 34–36], the dimensionless equations of the problem are expressed in the following form:

$$\frac{\partial^4 \psi}{\partial y^4} + N \frac{\partial^2 w}{\partial y^2} + \text{Re} S^2 (1 - N) \frac{\partial^3 \phi}{\partial y^3} = 0, \quad \frac{2 - N}{m^2} \frac{\partial^2 w}{\partial y^2} = 2w + \frac{\partial^2 \psi}{\partial y^2}, \tag{2.31}$$

$$\frac{\partial^2 \phi}{\partial y^2} = R_m \left(E - \frac{\partial \psi}{\partial y} \right). \tag{2.32}$$

Combining these equations gives

$$\psi = \frac{1}{H^2(1-N)}\left\{\frac{2-N}{m^2}\left(\frac{\partial^2 w}{\partial y^2} - m^2 w\right) + \eta y - C_1 y - C_2\right\},$$

$$\frac{\partial^4 w}{\partial y^4} - \left\{m^2 + H^2(1-N)\right\}\frac{\partial^2 w}{\partial y^2} + \frac{2m^2 H^2(1-N)}{2-N}w = 0,$$

(2.33)

where $H^2 = \mathrm{Re}S^2 R_m$, $H = (\mu_e H_0)a\sqrt{\sigma/\mu}$ is the Hartmann number (suitably greater than $\sqrt{2}$), $\eta = EH^2(1-N)$, and C_1, C_2 are an integration constants.

3. Exact solution

The general solutions of the microrotation component w and the stream function ψ are

$$w = A\cosh(\theta_1 y) + B\sinh(\theta_1 y) + C\cosh(\theta_2 y) + D\sinh(\theta_2 y),$$

$$\psi = \frac{1}{H^2(1-N)}\left\{\frac{2-N}{m^2}\left[(\theta_1^2 - m^2)(A\cosh(\theta_1 y) + B\sinh(\theta_1 y))\right.\right.$$

$$\left.\left. + (\theta_2^2 - m^2)(C\cosh(\theta_2 y) + D\sinh(\theta_2 y))\right] + \eta y - C_1 y - C_2\right\},$$

(3.1)

where

$$\theta_1 = \frac{1}{\sqrt{2}}\sqrt{((1-N)H^2 + m^2) + \sqrt{((1-N)H^2 + m^2)^2 - 4\left(\frac{2m^2(1-N)H^2}{(2-N)}\right)}},$$

$$\theta_2 = \frac{1}{\sqrt{2}}\sqrt{((1-N)H^2 + m^2) - \sqrt{((1-N)H^2 + m^2)^2 - 4\left(\frac{2m^2(1-N)H^2}{(2-N)}\right)}}.$$

(3.2)

Using the corresponding boundary conditions in (2.20), we get

$$A = 0, \qquad C = 0, \qquad C_2 = 0,$$

$$D = \frac{H^2 m^2}{(2-N)}\frac{(1-N)(F+h)}{\sinh(\theta_2 h)[\xi_2(1 - \theta_2 h\coth(\theta_2 h)) - \xi_1(1 - \theta_1 h\coth(\theta_1 h))]},$$

$$B = \frac{-H^2 m^2}{2-N}\frac{(1-N)(F+h)}{\sinh(\theta_1 h)[\xi_2(1 - \theta_2 h\coth(\theta_2 h)) - \xi_1(1 - \theta_1 h\coth(\theta_1 h))]},$$

(3.3)

$$C_1 = H^2(1-N)\left\{1 + \frac{(F+h)}{\zeta}(\theta_2\xi_2\coth(\theta_2 h) - \theta_1\xi_1\coth(\theta_1 h))\right\} + \eta,$$

$$\zeta = \xi_2(1 - \theta_2 h\coth(\theta_2 h)) - \xi_1(1 - \theta_1 h\coth(\theta_1 h)), \qquad \xi_i = \theta_i^2 - m^2, \quad i = 1, 2.$$

Thus the stream function and the microrotation component w will take the forms

$$\psi(x,y) = \frac{(F+h)}{\zeta} \left\{ \xi_2 \frac{\sinh(\theta_2 y)}{\sinh(\theta_2 h)} - \xi_1 \frac{\sinh(\theta_1 y)}{\sinh(\theta_1 h)} \right\}$$

$$- \left\{ 1 + \frac{(F+h)}{\zeta} (\theta_2 \xi_2 \coth(\theta_2 h) - \theta_1 \xi_1 \coth(\theta_1 h)) y \right\}, \tag{3.4}$$

$$w(x,y) = \frac{(F+h)(1-N)H^2 m^2}{(2-N)\zeta} \left\{ \frac{\sinh(\theta_2 y)}{\sinh(\theta_2 h)} - \frac{\sinh(\theta_1 y)}{\sinh(\theta_1 h)} \right\}.$$

Now solving (2.32) with the corresponding boundary conditions in (2.30), we get the magnetic force function in the form

$$\phi(x,y) = R_m \left\{ \frac{\xi_1(F+h)}{\theta_1 \zeta} \frac{\cosh(\theta_1 y)}{\sinh(\theta_1 h)} - \frac{\xi_2(F+h)}{\theta_2 \zeta} \frac{\cosh(\theta_2 y)}{\sinh(\theta_2 h)} \right.$$

$$\left. + \frac{y^2}{2} \left(1 + \frac{F+h}{\zeta} (\theta_2 \xi_2 \coth(\theta_2 h) - \theta_1 \xi_1 \coth(\theta_1 h)) + E \right) \right\} + C_3 y + C_4, \tag{3.5}$$

where

$$C_3 = 0,$$

$$C_4 = -R_m \left\{ \frac{\xi_1(F+h)}{\theta_1 \zeta} \frac{\cosh(\theta_1 h)}{\sinh(\theta_1 h)} - \frac{\xi_2(F+h)}{\theta_2 \zeta} \frac{\cosh(\theta_2 h)}{\sinh(\theta_2 h)} \right.$$

$$\left. - \frac{h^2}{2} \left(1 + \frac{(F+h)}{\zeta} (\theta_2 \xi_2 \coth(\theta_2 h) - \theta_1 \xi_1 \coth(\theta_1 h)) + E \right) \right\}. \tag{3.6}$$

Also, the axial-induced magnetic field and the current density distribution across the channel will take the forms

$$h_x(x,y) = R_m \left\{ \frac{\xi_1(F+h)}{\zeta} \frac{\sinh(\theta_1 y)}{\sinh(\theta_1 y)} - \frac{\xi_2(F+h)}{\zeta} \frac{\sinh(\theta_2 y)}{\sinh(\theta_2 h)} \right.$$

$$\left. + y \left(1 + \frac{F+h}{\zeta} (\theta_2 \xi_2 \coth(\theta_2 h) - \theta_1 \xi_1 \coth(\theta_1 h)) + E \right) \right\},$$

$$J_z(x,y) = R_m \left\{ \frac{\theta_1 \xi_1(F+h)}{\zeta} \frac{\cosh(\theta_1 y)}{\sinh(\theta_1 h)} - \frac{\theta_2 \xi_2(F+h)}{\zeta} \frac{\cosh(\theta_2 y)}{\sinh(\theta_2 h)} \right. \tag{3.7}$$

$$\left. + \left(1 + \frac{F+h}{\zeta} (\theta_2 \xi_2 \coth(\theta_2 h) - \theta_1 \xi_1 \coth(\theta_1 h)) + E \right) \right\}.$$

In the formulation under consideration, the field strength E is the determining factor and its value can be found by integrating (2.32), which represents Ohm's law in differential form, across the channel, taking into account the boundary conditions for ϕ and ψ in (2.30). In this case, we obtain the dimensionless $E = F/h$.

When the flow is steady in the wave frame, one can characterize the pumping performance by means of the the pressure rise per wavelength. So, the axial pressure gradient can be obtained from the equation

$$\frac{\partial p}{\partial x} = \frac{1}{(1-N)} \frac{\partial^3 \psi}{\partial y^3} + \frac{N}{1-N} \frac{\partial w}{\partial y} + H^2 \left(E - \frac{\partial \psi}{\partial y} \right). \tag{3.8}$$

Using (3.4), the axial pressure gradient will take the form

$$\begin{aligned}
\frac{\partial p}{\partial x} = \frac{(F+h)\theta_2}{\zeta} &\left\{ \xi_2 \left(\frac{\theta_2^2}{1-N} - H^2 \right) + \frac{NH^2 m^2}{2-N} \right\} \frac{\cosh(\theta_2 y)}{\sinh(\theta_2 h)} \\
&- \frac{(F+h)\theta_1}{\zeta} \left\{ \xi_1 \left(\frac{\theta_1^2}{1-N} - H^2 \right) + \frac{NH^2 m^2}{2-N} \right\} \frac{\cosh(\theta_1 y)}{\sinh(\theta_1 h)} \\
&+ H^2 \left\{ (E+1) - \frac{(F+h)}{\zeta} (\theta_1 \xi_1 \coth(\theta_1 h) - \theta_2 \xi_2 \coth(\theta_2 h)) \right\}.
\end{aligned} \tag{3.9}$$

The pressure rise Δp_λ for a channel of length L in its nondimensional forms is given by

$$\Delta p_\lambda = \int_0^1 \frac{\partial p}{\partial x} dx. \tag{3.10}$$

The integral in (3.10) is not integrable in closed form, it is evaluated numerically using a digital computer.

An interesting property of the micropolar fluid is that the stress tensor is not symmetric. The nondimensional shear stresses in the problem under consideration are given by

$$\begin{aligned}
\tau_{xy} &= \frac{\partial^2 \psi}{\partial y^2} - \frac{N}{1-N} w, \\
\tau_{yx} &= \left(\frac{1}{1-N} \right) \frac{\partial^2 \psi}{\partial y^2} + \frac{N}{1-N} w.
\end{aligned} \tag{3.11}$$

The shear stresses τ_{xy} and τ_{yx} are calculated at both the lower and upper walls and graphical results are shown in Figures 4–6.

4. Numerical results and discussion

This section is divided into three subsections. In the first subsection, the effects of various parameters on the pumping characteristics of a magneto-miropolar fluid are investigated. The magnetic field characteristics are discussed in the second subsection. The trapping phenomenon and the magnetic-force lines are illustrated in the last subsection.
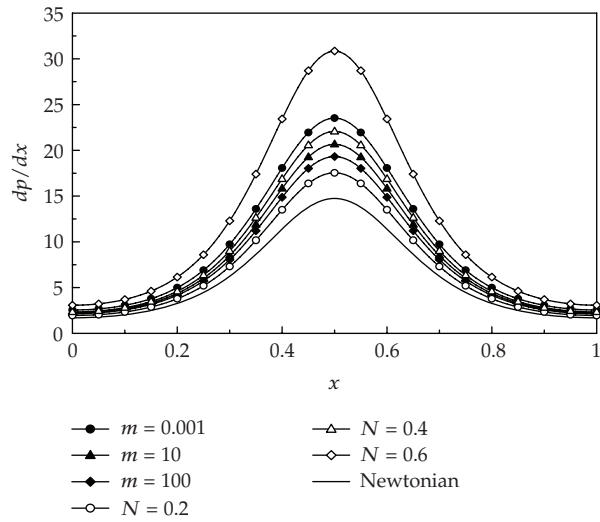
Figure 1: The axial pressure gradient versus the wavelength for $\alpha = 0.3$, $\theta = -1.2$, $H = 2$ and different values of m and N.
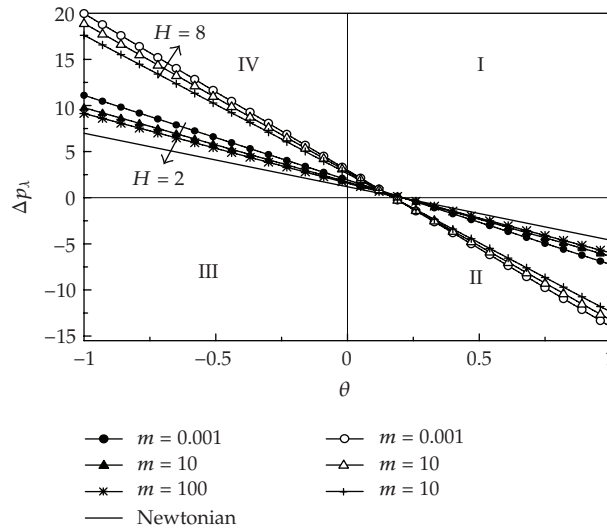
Figure 2: The pressure rise versus flow rate for $\alpha = 0.4$, $N = 0.4$, $H = 2$, and $H = 8$ at different values of m.

4.1. Pumping characteristics

This subsection describes the influences of various emerging parameters of our analysis on the axial pressure gradient $\partial p / \partial x$, the pressure rise per wavelength Δp_λ, and the shear stresses τ_{xy}, τ_{yx} on the lower and upper walls. The effects of these parameters are shown in Figures 1–6, and in most of the figures, the case of $N \to 0$ corresponds to that of Newtonian fluid.

Figure 1 illustrates the variation of the axial pressure gradient with x for different values of the microrotation parameter m and the coupling number N. We can see that in the
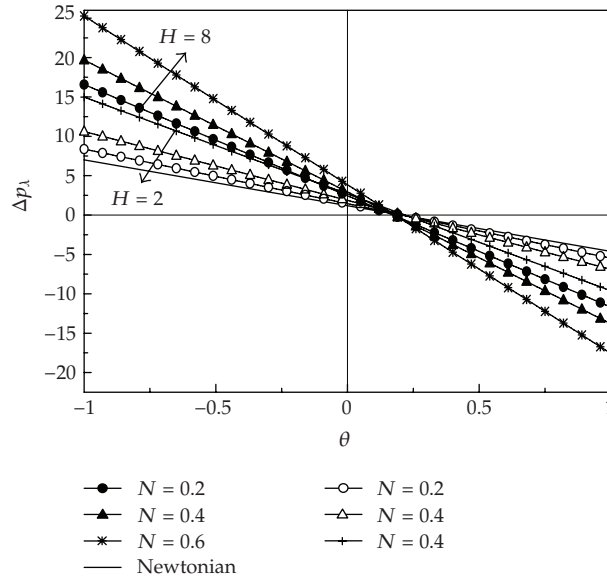
Figure 3: The pressure rise versus flow rate for $\alpha = 0.4$, $m = 2$, $H = 2$, and $H = 8$ at different values of N.
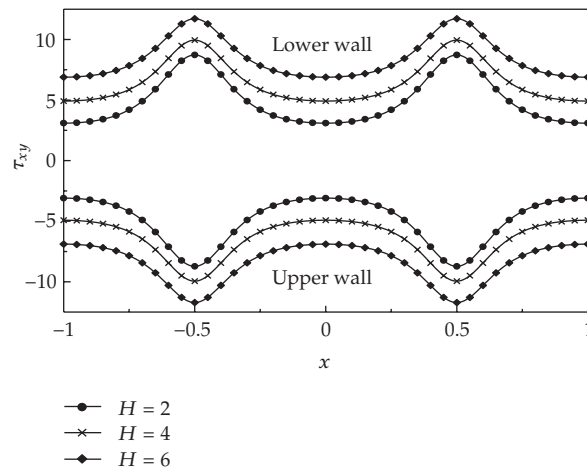
Figure 4: The shear stresses τ_{xy} for $\alpha = 0.5$, $\theta = 1.2$, $m = 3$, $N = 0.6$, and different values of H.

wider part of the channel $x \epsilon$ [0, 0.2] and [0.8,1.0], the pressure gradient is relatively small, that is, the flow can easily pass without imposition of large pressure gradient. Where, in a narrow part of the channel $x \epsilon$ [0.2, 0.8], a much larger pressure gradient is required to maintain the same flux to pass it, especially for the narrowest position near $x = 0.5$. This is in well agreement with the physical situation. Also from this figure, we observe the effect of m and N on the pressure gradient for fixed values of the other parameters, where the amplitude of dp/dx decrease as m increases and increases with increasing N, and the smallest value of such amplitude corresponds to the case $N \rightarrow 0$ (Newtonian fluid). The effect of the Hartmann number H on dp/dx is not included, where it is illustrated in a previous paper [44], where the amplitude of dp/dx increases as H increases.
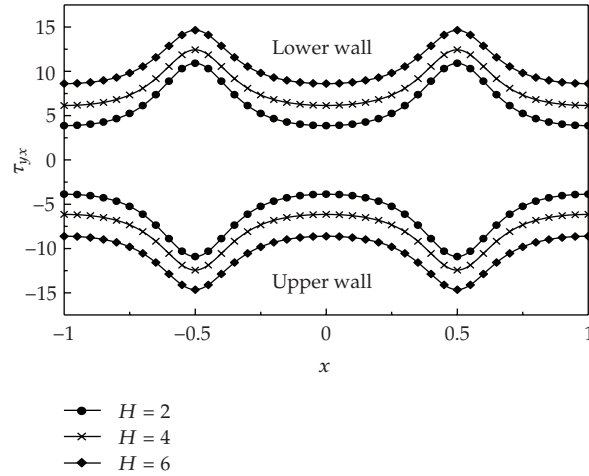
Figure 5: The shear stresses τ_{yx} for $\alpha = 0.5$, $\theta = 1.2$, $m = 3$, $N = 0.6$, and different values of H.
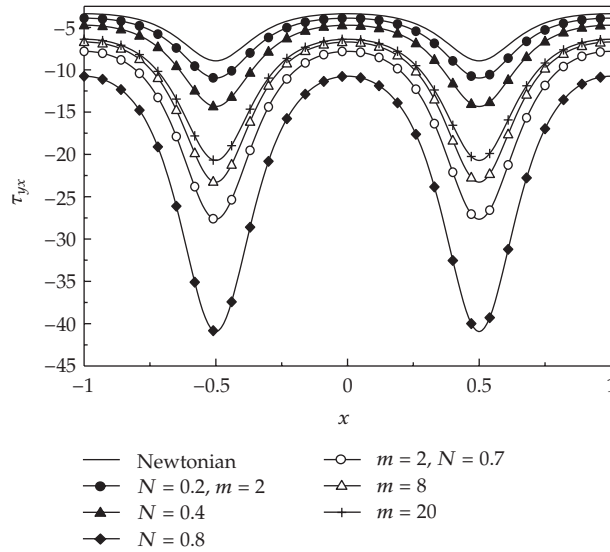
Figure 6: The shear stresses τ_{yx} for $\alpha = 0.5$, $\theta = 1.2$, $H = 3$, and different values of m and N.

Figures 2 and 3 illustrate the change of the pressure rise Δp_λ versus the time-averaged mean flow rate θ for various values of the parameters m (= 0.001, 10, 100 with $N = 0.4$, $\alpha = 0.4$ and different values of H) and N(= 0.2, 0.4, 0.6 with $m = 2$, $\alpha = 0.4$ and different values of H).

The graph is sectored so that the upper right-hand quadrant (I) denotes the region of peristaltic pumping, where $\theta > 0$ (positive pumping) and $\Delta p_\lambda > 0$ (adverse pressure gradient). Quadrant (II), where $\Delta p_\lambda < 0$ (favorable pressure gradient) and $\theta > 0$ (positive pumping), is designated as augmented flow (copumping region). Quadrant (IV), such that $\Delta p_\lambda > 0$ (adverse pressure gradient) and $\theta < 0$, is called retrograde or backward pumping. The flow is opposite to the direction of the peristaltic motion, and there is no flows in the
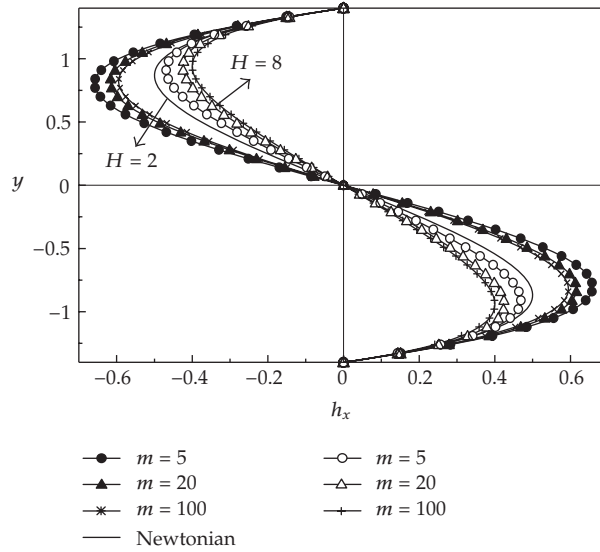
Figure 7: Variation of the axial-induced magnetic field across the channel for $\alpha = 0.4$, $\theta = 1.2$, $N = 0.9$, $R_m = 1$, and different values of m and H.
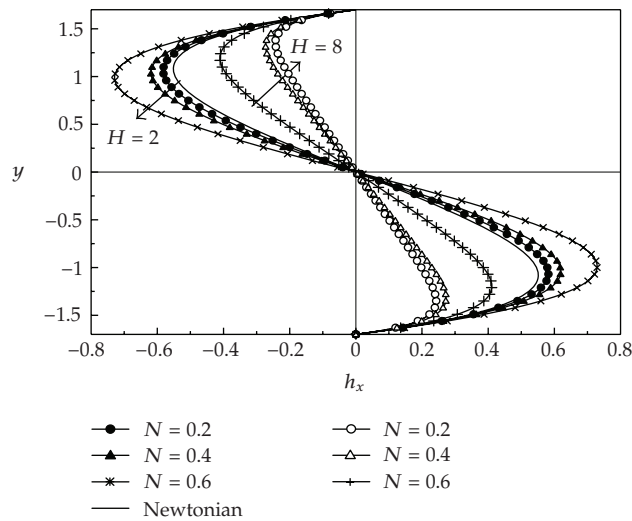
Figure 8: Variation of the axial-induced magnetic field across the channel for $\alpha = 0.4$, $\theta = 1.2$, $m = 2$, $R_m = 1$, and different values of N and H.

last quadrant (Quadrant (III)). It is shown in both Figures 2 and 3, that there is an inversely linear relation between Δp_λ and θ, that is, the pressure rise decreases with increasing the flow rate and the pumping curves are linear both for Newtonian and micropolar fluid. Moreover, the pumping curves for micropolar fluid lie above the Newtonian fluid in pumping region ($\Delta p_\lambda > 0$), but as m increases, the curves tend to coincide. In copumping region ($\Delta p_\lambda < 0$), the pumping increases with an increase in m. Figure 3 shows the effects of the coupling number N on Δp_λ, where the pumping increases with an increase in N and the pumping curve for
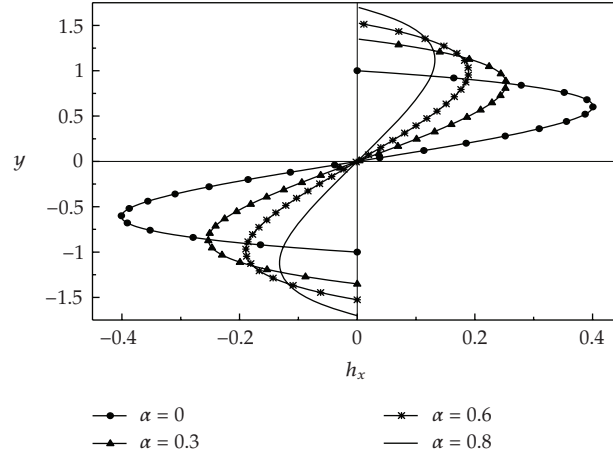
Figure 9: Variation of the axial-induced magnetic field across the channel for $m = 3$, $N = 0.6$, $H = 4$, $R_m = 2$, $\theta = -1.2$ and different values of α.
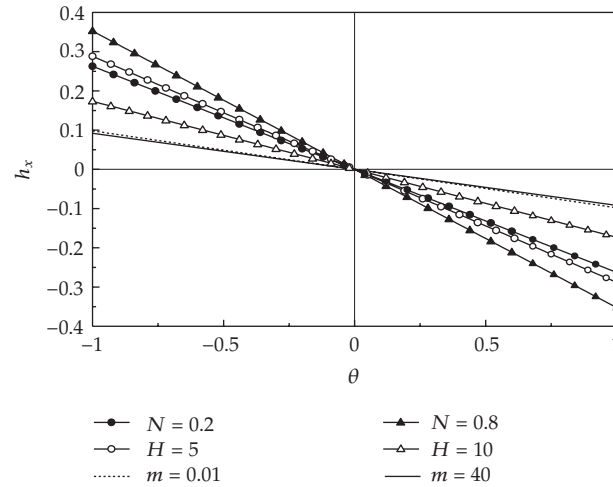
Figure 10: Axial-induced magnetic field versus flow rate for $\alpha = 0.5$ for different values of N at $m = 2$, $H = 4$, $R_m = 2$ for different values of m at $N = 0.7$, $H = 7$, $R_m = 1$, and for different values of H at $m = 4$, $N = 0.6$, $R_m = 2$.

the Newtonian fluid lies below the curves for micropolar fluid in the pumping region, and in the copumping region, the pumping decreases with an increase in N.

It is known that the stress tensor is not symmetric in micropolar fluid, that is why the expressions for τ_{xy} and τ_{yx} are different. In Figures 4 and 5, we have plotted the shear stresses τ_{xy} and τ_{yx} at the upper and lower walls for various values of the Hartmann number H. It can be seen that both shear stress are symmetric about the line $x = 0$. However, its magnitude increases as H increases. Moreover, both shear stresses have directions opposite to the upper wave velocity, while the directions of these shear stresses are along the direction of the lower wave velocity. Figure 6 indicates that the shear stress τ_{yx} decreases with an increase in the microrotation parameter m, while it increases as the coupling number N increases, and so,
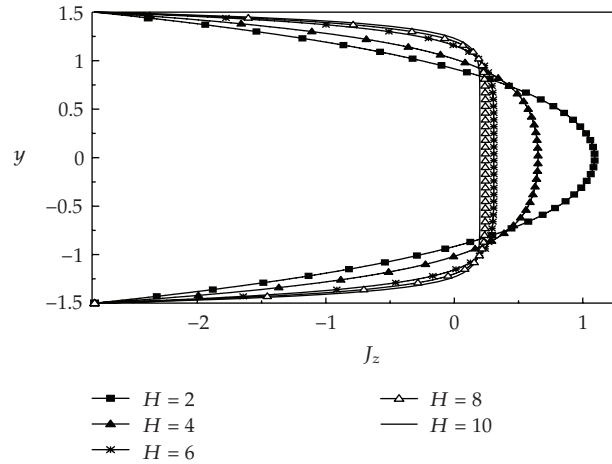
Figure 11: Variation of the current density distribution across the channel for $\alpha = 0.5$, $\theta = 1.6$, $m = 3$, $N = 0.2$, $R_m = 1$, and different values of H.
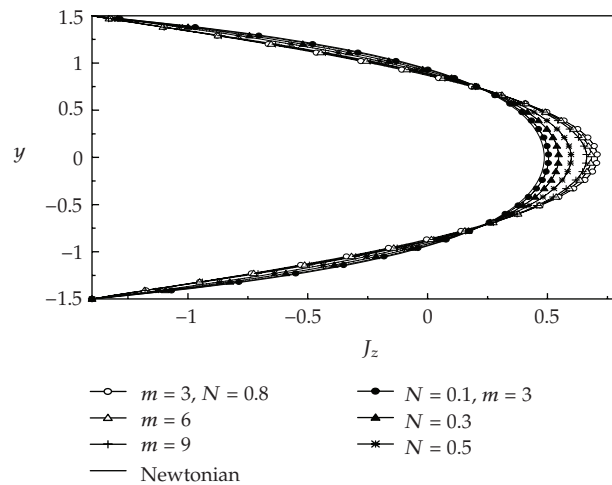
Figure 12: Variation of the current density distribution across the channel for $\alpha = 0.5$, $\theta = 1.6$, $H = 2$, $R_m = 1$, and different values of m and N.

the magnitude value of shear stress for a Newtonian fluid is less than that for a micropolar fluid.

4.2. Magnetic field characteristics

The variations of the axial-induced magnetic field h_x across the channel at $x = 0$ and the current density distribution J_z across the channel for various values of m, N, H, R_m, and α are displayed in Figures 7–12.

In Figures 7-8, m (= 5, 20, 100 with $N = 0.9$, $R_m = 1$, $\alpha = 0.4$ and $\theta = 1.2$ and different values of H), N (= 0.2, 0.4, 0.6 with $m = 2$, $R_m = 1$, $\alpha = 0.4$ and $\theta = 1.2$ and different values of H).
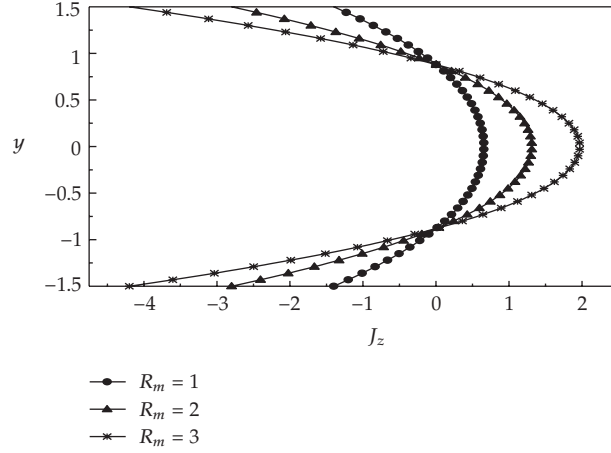
Figure 13: Variation of the current density distribution across the channel for $\alpha = 0.5$, $\theta = 1.6$, $H = 4$, $m = 3$, $N = 0.2$, and different values of R_m.

These figures indicate that the magnitude of the axial-induced magnetic field h_x decreases as the microrotation parameter m and the Hartmann number H increases while it increases as the coupling number N increases. Further in the half region, the induced magnetic field is one direction, and in the other half, it is in the opposite direction and it is zero at $y = 0$. Figure 9 illustrates the variation of h_x across the channel for different values of the amplitude ratio α at $x = 0.5$, where α (= 0, 0.3, 0.6, 0.9 with $m = 3$, $N = 0.6$, $H = 4$, $R_m = 2$, and $\theta = -1.2$). It is clear that the magnitude of the axial-induced magnetic field h_x at $\alpha = 0$ (no peristalsis) is larger, and it decreases with increasing α. The distributions of h_x within the time-averaged mean flow rate θ are exhibited in Figure 10 at $x = 0.25$, $y = 0.5$, where h_x is plotted for various values of the parameters N (= 0.2, 0.8 with $m = 2$, $H = 4$, $R_m = 2$, $\alpha = 0.5$), m (= 0.01, 40 with $N = 0.7$, $H = 7$, $R_m = 1$, $\alpha = 0.5$) and H (= 5, 10 with $m = 4$, $N = 0.6$, $R_m = 2$, $\alpha = 0.5$). From this figure, we observe that there is an inversely linear relation between h_x and θ for any value of the above-mentioned parameters, that is, h_x decreases with increasing the flow rate θ and that the obtained curves will intersect at the point $\theta = 0$. It is found also that for any value of $\theta \leq 0$, the effect of increasing each of M and H is to decrease h_x values whereas the effect of increasing N is to increase the value of h_x. On the other hand, for any value of $\theta \geq 0$, all the obtained lines will behave in an opposite manner to this behavior when $\theta \leq 0$.

Figures 11–13 describe the distribution of the current density J_z within y for different values of m, N, H, and R_m at the central line of the channel ($x = 0$), where H (= 2, 4, 6, 8, 10 with $m = 3$, $N = 0.2$, $R_m = 1$, $\alpha = 0.5$, $\theta = 1.6$), m (= 3, 6, 9 with $N = 0.8$, $H = 2$, $R_m = 1$, $\alpha = 0.5$ and $\theta = 1.6$), N (= 0.1, 0.3, 0.5 with $m = 3$, $H = 2$, $R_m = 1$, $\alpha = 0.5$ and $\theta = 1.6$), and R_m (= 1, 2, 3, with $m = 3$, $N = 0.2$, $H = 4$, $\alpha = 0.5$, $\theta = 1.6$). The graphical results of these figures indicate that the dimensionless current density J_z decreases as H and M increase in the region near the center of the channel while it increases for the same values of H and M in the region near to the lower and upper walls, that is, the net current flow through the channel is zero and this corresponds to the case of open circuit. However, an opposite behavior is noticed as N and R_m increases. Also, the current value for a micropolar fluid is higher than that for a Newtonian fluid.

(a)

(b)

(c)
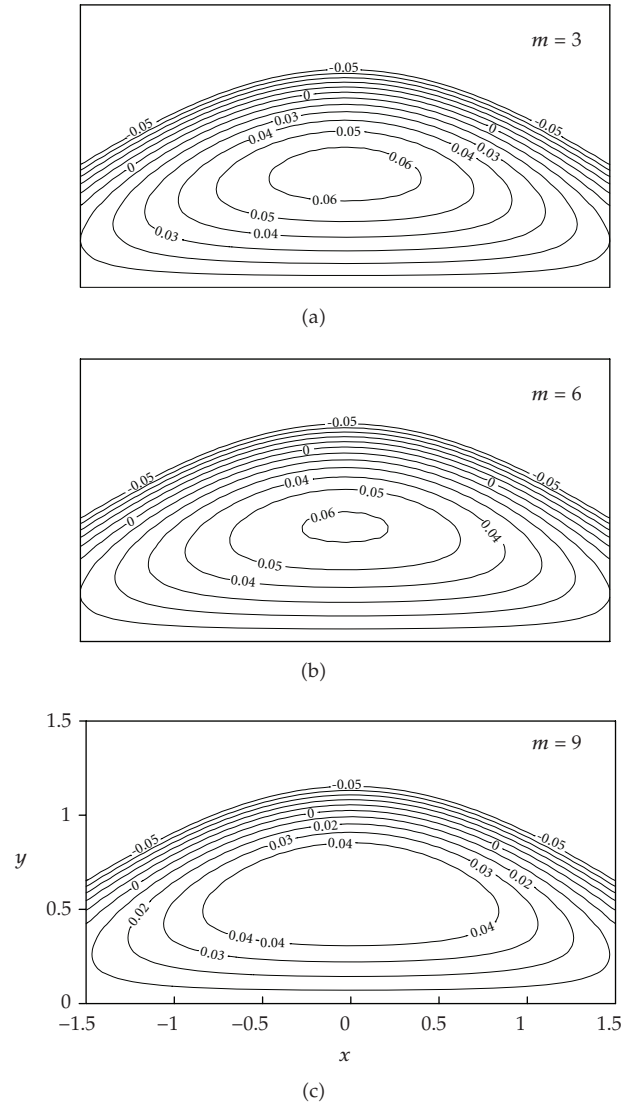
Figure 14: Stream lines for different values of *m*.

4.3. Trapping phenomena and magnetic-force lines

Another interesting phenomenon in peristaltic motion is trapping. In the wave frame, streamlines under certain conditions split to trap a bolus which moves as a whole with the speed of the wave. To see the effects of microrotation parameter *m* and the coupling number *N* on the trapping, we prepared Figures 14 and 15 for various values of the parameters *m* (= 3, 6, 9 with $N = 0.5$, $H = 2$, $\theta = 0.7$, $\alpha = 0.5$) and $N = (0.2, 0.4, 0.8$ with $m = 7$, $H = 2$, $\theta = 0.7$, $\alpha = 0.5$). Figures 14 and 15 reveal that the trapping is about the center line and the trapped bolus decrease in size as the microrotation parameter m increases, while the size of the bolus increases as *N* increases. Also the effects of *m* and *N* on the magnetic-force function ϕ are illustrated in Figures 16 and 17 for various values of the parameters

(a)

(b)

(c)
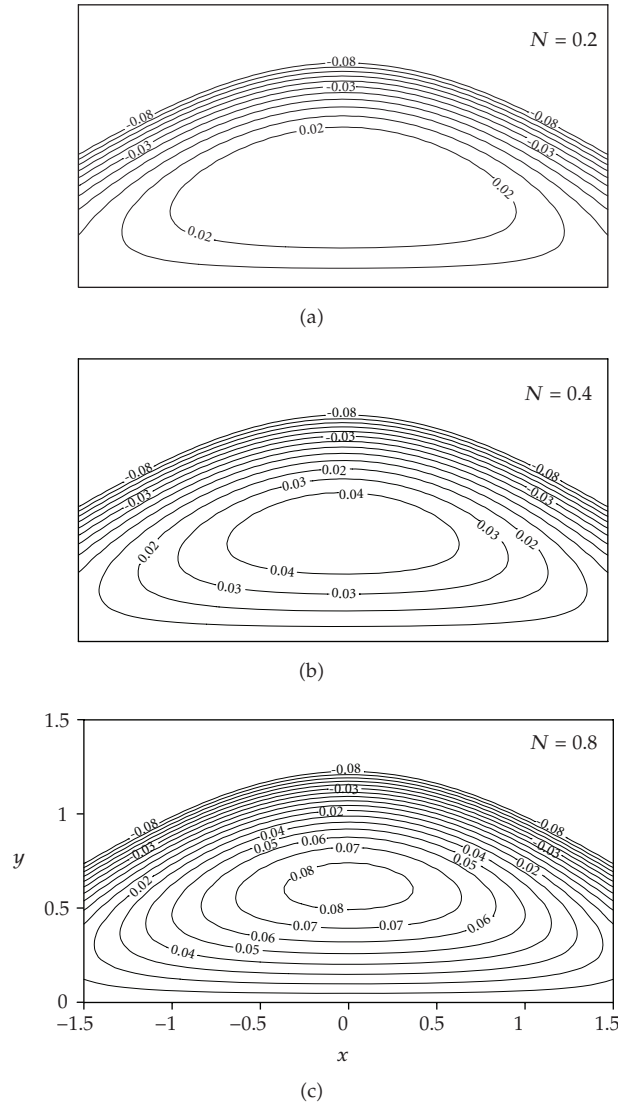
Figure 15: Stream lines for different values of N.

m (= 0.01, 3, 10, with $N = 0.5$, $H = 2$, $\theta = 0.7$, $R_m = 1$, $\alpha = 0.4$) and $N = (0.1, 0.4, 0.8$, with $m = 3$, $H = 2$, $\theta = 0.7$, $R_m = 1$, $\alpha = 0.4$). It is observed that as m increases, the size of the magnetic-force lines will decrease, and for large values of m, these lines will vanish at the center of the channel. An opposite behavior will occur as the coupling number N increase, where the width of the magnetic-force lines will increase and more magnetic-force lines will be created at the center of the channel as the coupling number N increases.

5. Concluding remarks

The effect of the induced magnetic field on peristaltic flow of a magneto-micropolar fluid is studied. The exact expressions for stream function, magnetic-force function, axial

(a)

(b)

(c)
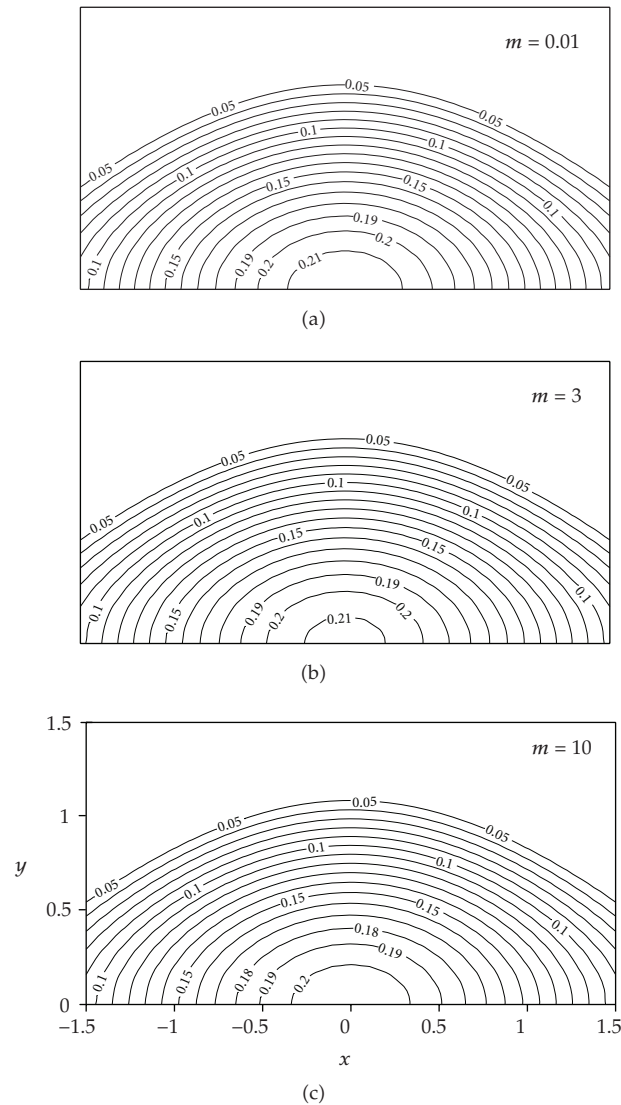
Figure 16: Magnetic-force lines for different values of m.

pressure gradient, axial-induced magnetic field, and current density are obtained analytically. Graphical results are presented for the pressure rise per wave length, shear stresses on the lower and upper walls, axial-induced magnetic field, and current density and trapping. The main findings can be summarized as follows.

(1) The value of the axial pressure gradient dp/dx is higher for a magneto-micropolar fluid than that for a Newtonian fluid.

(2) The magnitude of pressure rise per wavelength for a magneto-micropolar fluid is greater than that of a Newtonian fluid in the pumping region, while in the copumping region, the situation is reversed.
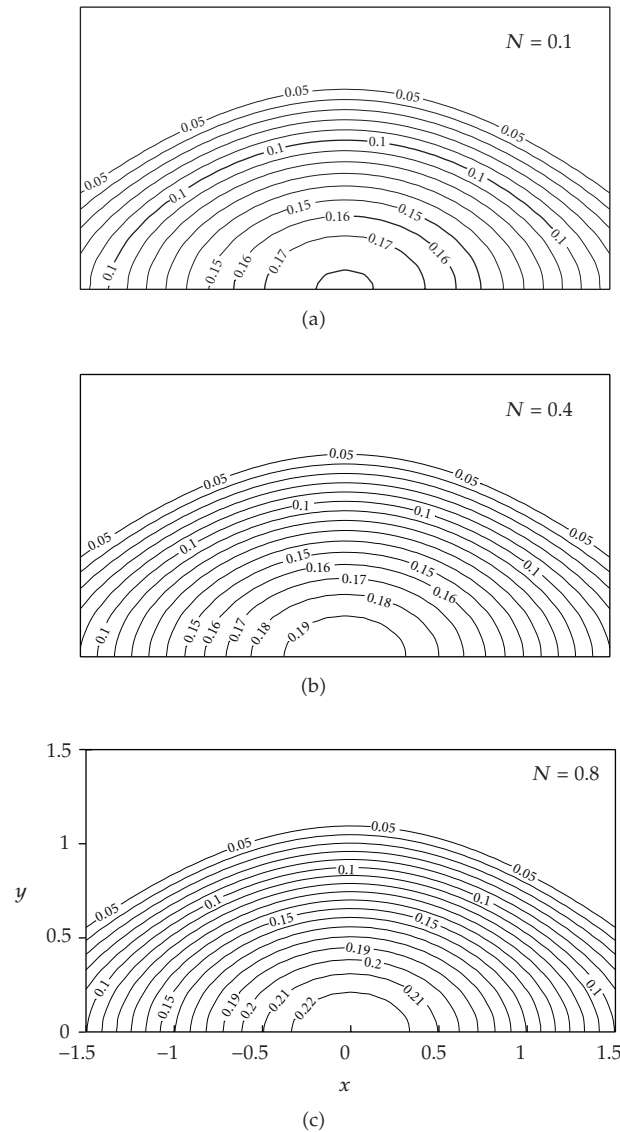
Figure 17: Magnetic-force lines for different values of N.

(3) Shear stresses at the lower wall are quite similar to those for the upper wall except that at the upper wall has its direction opposite to the upper wave velocity while at the lower wall has its direction along the wave velocity.

(4) The shear stresses decrease with an increase of m and increases with increasing N.

(5) The axial-induced magnetic field is higher for a Newtonian fluid than that for a micropolar fluid and smaller as the transverse magnetic field increases.

(6) There is an inversely linear relation between the axial-induced magnetic field and the flow rate.

(7) The current density J_z at the center of the channel is higher for a micropolar fluid than that for a Newtonian fluid, and it will decrease as the microrotation parameter and transverse magnetic field increases, while it increases as the coupling number increases.

(8) As we move from the Newtonian fluid to a micropolar fluid, more trapped bolus created at the center line and the size of these bolus increases.

(9) More magnetic force lines created at the center of the channel as the fluid moves from Newtonian fluid to a micropolar fluid.

References

[1] K. K. Raju and R. Devanathan, "Peristaltic motion of a non-Newtonian fluid," *Rheologica Acta*, vol. 11, no. 2, pp. 170–178, 1972.

[2] G. Böhme and R. Friedrich, "Peristaltic flow of viscoelastic liquids," *Journal of Fluid Mechanics*, vol. 128, pp. 109–122, 1983.

[3] L. M. Srivastava and V. P. Srivastava, "Peristaltic transport of blood: Casson model—II," *Journal of Biomechanics*, vol. 17, no. 11, pp. 821–829, 1984.

[4] Kh. S. Mekheimer, "Peristaltic transport of a couple stress fluid in a uniform and non-uniform channels," *Biorheology*, vol. 39, no. 6, pp. 755–765, 2002.

[5] N. Ali, T. Hayat, and M. Sajid, "Peristaltic flow of a couple stress fluid in an asymmetric channel," *Biorheology*, vol. 44, no. 2, pp. 125–138, 2007.

[6] Kh. S. Mekheimer and Y. Abd Elmaboud, "Peristaltic flow of a couple stress fluid in an annulus: application of an endoscope," *Physica A*, vol. 387, no. 11, pp. 2403–2415, 2008.

[7] A. C. Eringen, *Microcontinuum Field Theories. II. Fluent Media*, Springer, New York, NY, USA, 2001.

[8] D. Philip and P. Chandra, "Peristaltic transport of simple microfluid," *Proceedings of the National Academy of Sciences, India. Section A*, vol. 65, no. 1, pp. 63–74, 1995.

[9] P. Muthu, B. V. Rathish Kumar, and P. Chandra, "On the influence of wall properties in the peristaltic motion of micropolar fluid," *The ANZIAM Journal*, vol. 45, no. 2, pp. 245–260, 2003.

[10] T. Hayat, N. Ali, and Z. Abbas, "Peristaltic flow of a micropolar fluid in a channel with different wave forms," *Physics Letters A*, vol. 370, no. 3-4, pp. 331–344, 2007.

[11] A. C. Eringen, "Theory of micropolar fluids," *Journal of Mathematics and Mechanics*, vol. 16, pp. 1–18, 1966.

[12] R. Girija Devi and R. Devanathan, "Peristaltic transport of micropolar fluid," *Proceedings of the National Academy of Sciences, India. Section A*, vol. 81, pp. 149–163, 1975.

[13] K. P. Selverov and H. A. Stone, "Peristaltically driven channel flows with applications toward micromixing," *Physics of Fluids*, vol. 13, no. 7, pp. 1837–1859, 2001.

[14] Abd El Hakeem Abd El Naby and A. E. M. El Misiery, "Effects of an endoscope and generalized Newtonian fluid on peristaltic motion," *Applied Mathematics and Computation*, vol. 128, no. 1, pp. 19–35, 2002.

[15] T. Hayat, Y. Wang, A. M. Siddiqui, K. Hutter, and S. Asghar, "Peristaltic transport of a third-order fluid in a circular cylindrical tube," *Mathematical Models & Methods in Applied Sciences*, vol. 12, no. 12, pp. 1691–1706, 2002.

[16] T. Hayat, Y. Wang, A. M. Siddiqui, and K. Hutter, "Peristaltic motion of a Johnson-Segalman fluid in a planar channel," *Mathematical Problems in Engineering*, no. 1, pp. 1–23, 2003.

[17] Abd El Hakeem Abd El Naby, A. E. M. El Misery, and M. F. Abd El Kareem, "Separation in the flow through peristaltic motion of a carreau fluid in uniform tube," *Physica A*, vol. 343, no. 1–4, pp. 1–14, 2004.

[18] T. Hayat and N. Ali, "On mechanism of peristaltic flows for power-law fluids," *Physica A*, vol. 371, no. 2, pp. 188–194, 2006.

[19] T. Hayat, N. Ali, and S. Asghar, "Peristaltic motion of a Burger's fluid in a planar channel," *Applied Mathematics and Computation*, vol. 186, no. 1, pp. 309–329, 2007.

[20] T. Hayat, N. Ali, and S. Asghar, "An analysis of peristaltic transport for flow of a Jeffrey fluid," *Acta Mechanica*, vol. 193, no. 1-2, pp. 101–112, 2007.

[21] N. Ali and T. Hayat, "Peristaltic motion of a Carreau fluid in an asymmetric channel," *Applied Mathematics and Computation*, vol. 193, no. 2, pp. 535–552, 2007.

[22] M. H. Haroun, "Effect of Deborah number and phase difference on peristaltic transport of a third-order fluid in an asymmetric channel," *Communications in Nonlinear Science and Numerical Simulation*, vol. 12, no. 8, pp. 1464–1480, 2007.

[23] M. H. Haroun, "Non-linear peristaltic flow of a fourth grade fluid in an inclined asymmetric channel," *Computational Materials Science*, vol. 39, no. 2, pp. 324–333, 2007.

[24] V. C. A. Ferraro, *An Introduction to Magneto-Fluid Mechanics*, Clarendon Press, Oxford, UK, 1966.

[25] V. K. Stud, G. S. Sephon, and R. K. Mishra, "Pumping action on blood flow by a magnetic field," *Bulletin of Mathematical Biology*, vol. 39, no. 3, pp. 385–390, 1977.

[26] L. M. Srivastava and R. P. Agrawal, "Oscillating flow of a conducting fluid with a suspension of spherical particles," *Journal of Applied Mechanics*, vol. 47, pp. 196–199, 1980.

[27] H. L. Agrawal and B. Anwaruddin, "Peristaltic flow of blood in a branch," *Ranchi University Mathematical Journal*, vol. 15, pp. 111–121, 1984.

[28] Kh. S. Mekheimer, "Non-linear peristaltic transport of magnetohydrodynamic flow in an inclined planar channel," *Arabian Journal for Science and Engineering*, vol. 28, no. 2A, pp. 183–201, 2003.

[29] Kh. S. Mekheimer and T. H. Al-Arabi, "Nonlinear peristaltic transport of MHD flow through a porous medium," *International Journal of Mathematics and Mathematical Sciences*, vol. 2003, no. 26, pp. 1663–1682, 2003.

[30] Kh. S. Mekheimer, "Peristaltic flow of blood under effect of a magnetic field in a non-uniform channels," *Applied Mathematics and Computation*, vol. 153, no. 3, pp. 763–777, 2004.

[31] M. Elshahed and M. H. Haroun, "Peristaltic transport of Johnson-Segalman fluid under effect of a magnetic field," *Mathematical Problems in Engineering*, vol. 2005, no. 6, pp. 663–677, 2005.

[32] T. Hayat, F. M. Mahomed, and S. Asghar, "Peristaltic flow of a magnetohydrodynamic Johnson-Segalman fluid," *Nonlinear Dynamics*, vol. 40, no. 4, pp. 375–385, 2005.

[33] Abd El Hakeem Abd El Naby, A. E. M. El Misery, and M. F. Abd El Kareem, "Effects of a magnetic field on trapping through peristaltic motion for generalized Newtonian fluid in channel," *Physica A*, vol. 367, pp. 79–92, 2006.

[34] T. Hayat and N. Ali, "Peristaltically induced motion of a MHD third grade fluid in a deformable tube," *Physica A*, vol. 370, no. 2, pp. 225–239, 2006.

[35] T. Hayat, A. Afsar, M. Khan, and S. Asghar, "Peristaltic transport of a third order fluid under the effect of a magnetic field," *Computers & Mathematics with Applications*, vol. 53, no. 7, pp. 1074–1087, 2007.

[36] T. Hayat and N. Ali, "A mathematical description of peristaltic hydromagnetic flow in a tube," *Applied Mathematics and Computation*, vol. 188, no. 2, pp. 1491–1502, 2007.

[37] T. Hayat, M. Khan, A. M. Siddiqui, and S. Asghar, "Non-linear peristaltic flow of a non-Newtonian fluid under effect of a magnetic field in a planar channel," *Communications in Nonlinear Science and Numerical Simulation*, vol. 12, no. 6, pp. 910–919, 2007.

[38] Kh. S. Mekheimer and Y. Abd Elmaboud, "The influence of heat transfer and magnetic field on peristaltic transport of a Newtonian fluid in a vertical annulus: application of an endoscope," *Physics Letters A*, vol. 372, no. 10, pp. 1657–1665, 2008.

[39] T. Hayat, N. Ali, and S. Asghar, "Hall effects on peristaltic flow of a Maxwell fluid in a porous medium," *Physics Letters A*, vol. 363, no. 5-6, pp. 397–403, 2007.

[40] N. Ali, Q. Hussain, T. Hayat, and S. Asghar, "Slip effects on the peristaltic transport of MHD fluid with variable viscosity," *Physics Letters A*, vol. 372, no. 9, pp. 1477–1489, 2008.

[41] Y. Wang, T. Hayat, N. Ali, and M. Oberlack, "Magnetohydrodynamic peristaltic motion of a Sisko fluid in a symmetric or asymmetric channel," *Physica A*, vol. 387, no. 2-3, pp. 347–362, 2008.

[42] V. I. Vishnyakov and K. B. Pavlov, "Peristaltic flow of a conductive liquid in a transverse magnetic field," *Magnetohydrodynamics*, vol. 8, no. 2, pp. 174–178, 1972.

[43] N. T. M. Eldabe, M. F. El-Sayed, A. Y. Galy, and H. M. Sayed, "Peristaltically induced transport of a MHD biviscosity fluid in a non-uniform tube," *Physica A*, vol. 383, no. 2, pp. 253–266, 2007.

[44] Kh. S. Mekheimer, "Effect of the induced magnetic field on peristaltic flow of a couple stress fluid," *Physics Letters A*, vol. 372, no. 23, pp. 4271–4278, 2008.